NASA CR-177849

(NASA-CR-177849) GEOMAGNETIC MAIN FIELD MODELING USING MAGNETOHYDRODYNAMIC CONSTRAINTS (Business and Technological Systems, Inc.) 33 p HC A03/MF A01 CSCL 08G

N86-20997

Unclas
G3/46 05679

BTS

BTS03-85-51/k1
1080

November 1985

GEOMAGNETIC MAIN FIELD MODELING USING MAGNETOHYDRODYNAMIC CONSTRAINTS

by

Ronald H. Estes

prepared for

NASA/GODDARD SPACE FLIGHT CENTER
Greenbelt, Maryland 20771

under

Contract NAS5-28671

prepared by

BUSINESS AND TECHNOLOGICAL SYSTEMS, INC.
Aerospace Building, Suite 440
10210 Greenbelt Road
Seabrook, Maryland 20706

Acknowledgement

The work performed under this contract is the result of a joint but separately funded effort between Edward Benton of the University of Colorado, Ronald Estes of BTS and Robert Langel at the NASA/Goddard Space Flight Center. Theoretical aspects of the problem are funded under NASA/Goddard Contract NAS5-28670 to the University of Colorado under the direction of Dr. Benton while algorithmic development and computation are funded under NASA/ Goddard Space Flight Center Contract NAS5-28671 to Business and Technological Systems, Inc. Dr. Langel serves as a co-investigator to the joint project.

TABLE OF CONTENTS

1.0 INTRODUCTION

The objective of the study described in this report is to investigate the influence of physical constraints which may be approximately satisfied by the Earth's liquid core on models of the geomagnetic main field and its secular variation. A previous report (Estes, 1984) describes the methodology used to incorporate non-linear equations of constraint into the main field model, and will be referred to as Report I. This report describes the application of that methodology to the GSFC 12/83 field model (Langel and Estes, 1985a) to test the frozen-flux hypothesis and the usefulness of incorporating magnetohydrodynamic constraints for obtaining improved geomagnetic field models.

The geomagnetic field is a highly complex phenomenon with significant spatial and temporal variations. Global satellite surveys such as POGO and MAGSAT have led to important advances in our understanding of this global geophysical phenomenon and its applications in geology, tectonophysics, navigation, communications, and many other fields. The geomagnetic field is composed of three major components:

- The core field is the major part of the geomagnetic field and is believed to be caused by fluid motion of conducting material in the Earth's outer core. The field variations have large amplitudes, broad spatial features (i.e., wavelengths on the order of 1000 km and longer at the earth's surface), and significant low-frequency temporal variation.

- The crustal anomaly field forms a relatively small part of the geomagnetic field, but is significant since it is caused by geologic structure and the state of crustal minerals. The spatial variations of the crustal field occur with characteristic wavelengths ranging up to a few thousand km.

- The external field is caused by electrical currents in the ionosphere and magnetosphere. Magnetic field variations due to the external field occur on all spatial and temporal scales. The external field accounts for the most complex and dynamic part of the geomagnetic field.

Models of the main, or core field are required for a number of uses, including the production of declination charts for navigation, the removal of background fields from aeromagnetic and ship-borne magnetic surveys, satellite attitude control and determination, the probing of various fluid motions in the Earth's core, and calculations of field lines and conjugate points for ionospheric and magnetospheric studies. The geomagnetic secular variation has been demonstrated to be correlated with decade fluctuations in the Earth's rotation, and improved models could lead to better understanding of the nature of the core/mantle coupling. Moreover, knowledge of the secular variation of the core field is crucial in tying together regional aeromagnetic and marine surveys taken at different epochs. The secular variation is one of the few sources of information regarding the Earth's core, where the internal field originates.

As indicated above, the anomaly portion of the field arises from variably magnetized rocks lying between the Earth's surface and the Curie isotherm (the "magnetic crust"), and is the part of the magnetic field having direct geologic significance. The magnetic anomaly fields, which are essentially time independent for our purpose, have long been used to study near-surface geology and structure. They have had an important role in the initial evidence for sea-floor spreading that led to our present unifying concepts of plate tectonics and they are routinely used in resource exploration. Models of the sources of magnetic anomalies are the basis for geologic interpretation.

The modeling of the main and anomalous fields with high resolution is of major importance for earth science applications. In order to achieve this resolution, techniques for developing core and crustal models must be improved. Separating the core field from the crustal field is a major problem. Conventional approaches to representing the main field by a

truncated spherical harmonic series suffer from aliasing due to the crustal field above approximately degree and order twelve (Langel and Estes, 1982). This problem is described in detail by Langel (1985). A consequence of this is that extrapolation of main field models to the core/mantle boundary (CMB) is severly contaminated by the attenuated higher harmonic coefficients which are aliased by crustal influences. New approaches to this problem by Gubbins (1983, 1984) and Gubbins and Bloxham (1985) using a priori spectral assumptions and by Shure et. al. (1982) using harmonic splines minimizing a smoothness norm for the field at the CMB are important contributions. Currently, Langel and Estes (1985b) are investigating the separability problem through a correlated measurement noise weight matrix approach.

In addition to the ambiguity inherent in the separation process which imposes a fundamental limitation on accuracy, there is further difficulty in resolving the non-static nature of the main field. The main field changes in time on scales ranging from seconds to hundreds of thousands of years. Magnetic polarity reversals, for example, can take place over a period of a few thousand years, while tens to hundreds of thousands of years elapse between reversals. The interest of our study, however, is on magnetic variations over the scale of several decades and less. The secular variation (SV), even over those time scales, is less well known than the main field. This is due primarily to data availability. While the dense global vector magnetic survey provided by Magsat (Langel et. al, 1980) has permitted an excellent global "snapshot view" of the main field at epoch 1980, secular variation models depend principally on the data from the global network of permanent magnetic observatories which are few in number and poorly distributed. An additional difficulty is that magnetic features of smaller spatial scale are probably capable of more rapid temporal variation so that higher degree terms of the spherical harmonic series representation of the secular variation may be more important and convergence of the series weaker than that for the constant part of the main field. The result is that with current methods of modeling the main field and its secular variation even the large scale components of the geomagnetic field cannot be predicted into the future by more than a few years beyond the data span which defined the model. Two approaches are possible to improve the situation; to incorporate some statistical information

describing the SV process into the model (Gibbs and Estes, 1982, 1984), or to insert physical constraints provided by the electromagnetism and fluid dynamics of the source region, earth's outer core.

The work presented in this report describes the research accomplished in the second year of a multi-year study of the influence of magnetohydrodynamic constraints from the core on geomagnetic models, which is a joint effort between Edward Benton of the University of Colorado and Business and Technological Systems, Inc. Some theoretical aspects of the problem are presented by Benton (1984, 1985) in separate reports. As described in Report I, the BTS contribution in the first year was devoted to establishing appropriate geomagnetic data bases, establishing algorithms for incorporating non-linear constraints into the estimation procedure, and developing and verifying software based on these algorithms for computation. The demonstration that geomagnetic observations are consistent with the field being frozen to the core fluid has great importance for computing properties of the fluid core velocities, and for constructing improved predictive models. Gubbins (1984) and Bloxham and Gubbins (1985) have investigated the consistency of the observed data with frozen-flux constraints by two methods; they developed models that were forced to satisfy the flux constraints and then examined for acceptability the resulting misfit to the data used in the model, and they computed the flux integrals from unconstrained models at different epochs and compared their differences with formal error estimates from the models at the core surface. Our approach in this study uses the methodology of Report I to produce a constrained geomagnetic model based on GSFC (12/83) using the constraint equations as additional "data" with an associated uncertainty, and compares the misfit errors for data beyond the time interval defining the model (prediction errors) with those of the unconstrained model.

2.0 PHYSICAL CONSTRAINTS FOR MAIN FIELD MODELS

In the earth's core the geomagnetic field satisfies the induction equation

$$\dot{\underline{B}} = \nabla \times (\underline{V} \times \underline{B}) + \eta \nabla^2 \underline{B} \qquad (1)$$

where $\underline{B}$ is the vector field, $\underline{V}$ is the flow velocity and η is the magnetic diffusivity. On the time scale of a few decades, it has been shown to be a good approximation to ignore magnetic diffusion in the core (Backus, 1968), so that the core fluid is assumed to behave like a perfect conductor with the magnetic flux frozen into the fluid motion. Moreover, it is a reasonable first order approximation to treat the mantle as a perfect insulator. Horizontal components of $\underline{B}$ may be discontinuous across the CMB, but the radial component, B_r, must be continuous. Bondi and Gold (1950) introduced the scalar relation for the absolute unsigned magnetic flux, or "pole-strength"

$$M(r, t) = \int_0^{2\pi} \int_0^{\pi} \left| B_r(r, \theta, \lambda, t) \right| r^2 \sin\theta \, d\theta d\lambda \qquad (2)$$

as a measure of the number of field lines which cross the spherical surface of radius r at time t. They noted that the number of field lines crossing the top surface of a perfectly conducting core (CMB) is a constant of the motion. Then

$$M(b, t) = M_0 = \text{constant} \qquad (3)$$

is a scalar constraint for the frozen-flux hypothesis, where b is the radius of the CMB. Voorhies and Benton (1982) show that this constraint appears to be well satisfied, which provides support for the perfect conducting core/insulating mantle hypothesis over short time scales. Moreover, Backus (1968) has shown that the total absolute flux linking the CMB is the sum of contributions arising from separate "null-flux" patches, which are regions on the CMB bounded by contours of zero radial field. Denoting the contour of the i^{th} null-flux curve as Γ_i, then

$$M_i(b,\ t) = \int\int_{\Gamma_i} B_r(b,\ \theta,\ \lambda,\ t)\ b^2 \sin\theta\ d\theta d\lambda \qquad (4)$$

$$= \text{constant}$$

provide additional scalar integral constraints. Unfortunately, the null curves Γ_i are non-linear functions of the geomagnetic Gauss coefficients and, moreover, depend strongly on the truncation level of the spherical harmonic series for B_r.

Benton (1984, 1985) has pursued additional physical constraints on secular variation arising from the coupling of non-dissipative fluid dynamics to the frozen-flux electromagnetism of earth's core. He shows that the signed flux through any patch which is bounded by a curve which moves with the fluid should be conserved in the limit of perfect core conductivity, and examines possible candidates. He demonstrates that under some assumptions, for example, lines of absolute vorticity move with the fluid, and the contours on which the vertical absolute vorticity vanishes move with the fluid. A consequence of this is that under the stated assumptions (spherical, perfectly conducting inviscid core free of vertical Lorentz torque at the CMB) the geomagnetic flux through the northern geographic hemisphere on the core-mantle boundary (CMB) should be constant. With the assumption that the mantle is an insulator, the resulting constraint equation

$$L_E = \int_0^{2\pi} \int_0^{\pi/2} B_r(b,\ \theta,\ \phi,\ t)\ b^2 \sin\theta\ d\theta d\phi$$

$$= \sum_{n=1}^{N} \sqrt{\frac{n+1}{2n}} \left(\frac{a}{b}\right)^{n+2} g_n^0(t)\ P_n^1\left(\frac{\pi}{2}\right) = \text{const.} \qquad (5)$$

is linear in the Gauss coefficients g_{nm}. Here a is the Earth's radius, b is the radius of the CMB, and P_n^1 is the Schmidt normalized Legendre polynomial of degree n and order 1. Denoting

$$L_E = \sum_{m=1}^{N} F_n \, g_n^0(t) = \text{constant}$$

we have

$$F_n = -\frac{(n-2)}{(n-1)} \left(\frac{a}{b}\right)^2 F_{n-2}$$

where $F_0 = 0$ and $F_1 = 1$. Note that this represents a constraint equation for secular variation

$$\dot{L}_E = \sum_{n=1}^{N} F_n \, \dot{g}_n^0(t) = 0 \qquad (6)$$

which may be readily tested against existing models or easily incorporated as a linear constraint into a model.

Under the assumptions which established the flux linking the northern geographic hemisphere as a constant, additional flux constraints may be established for areas bounded by curves defined by the intersection of the geographic equator with the null curve along the geomagnetic equator on the CMB. These constraints, like those due to the frozen flux through the null curves, are non-linear functions of the Gauss coefficients and must be implemented numerically.

3.0 BAYESIAN LEAST SQUARES PARAMETER ESTIMATION

The Bayesian parameter estimation algorithm provides a methodology for including a priori statistical information on the parameter space in obtaining least squares solutions (Luenberger, 1973). Let x denote the parameter vector, y the measurement vector and ν represent the random noise vector with zero mean and covariance matrix R. Then the observation equation is

$$y = F(x) + \nu \quad . \tag{7}$$

In the linear case, assume $F(x) = Ax$ so that

$$y = Ax + \nu \quad . \tag{8}$$

Then if $\hat{x}_a$ denotes an a priori estimate of the parameters with a priori covariance matrix Ω_a, the estimate for the parameter state vector $\hat{x}$ is

$$\hat{x} = (A^T R^{-1} A + \Omega_a^{-1})^{-1} [A^T R^{-1} y + \Omega_a^{-1} \hat{x}_a] \quad . \tag{9}$$

This result may be obtained by minimizing the norm

$$J_{LS}(x) = (y - Ax)^T R^{-1} (y - Ax) + (x - \hat{x}_a)^T \Omega_a^{-1} (x - \hat{x}_a) \tag{10}$$

with respect to x, so that it is clear that the a priori information is included in the formalism as additional data.

For the non-linear problem, an iterative approach is required. Linearizing about a nominal solution x_0, we have

$$F(x) - F(x_0) = A(x_0)(x - x_0) + ... \quad . \tag{11}$$

A Gauss iteration procedure yields the equation for the $(n+1)^{st}$ approximation to the solution estimate where

$$\hat{x}_{n+1} = \hat{x}_n + \delta\hat{x}_{n+1} \tag{12}$$

$$\delta\hat{x}_{n+1} = (A^T(\hat{x}_n)\, R^{-1}A(\hat{x}_n) + \Omega_a^{-1})^{-1}\, [A^T(\hat{x}_n)\, R^{-1}\delta y_n + \Omega_a^{-1}[\hat{x}_a - \hat{x}_n]]$$

and

$$\delta y_n = y - A(\hat{x}_n)\, \hat{x}_n \quad .$$

The rate of convergence of the procedure depends on how good the nominal guess x_0 is, and on the non-linear character of the function $F(x)$. For highly non-linear problems, other techniques utilizing higher order derivatives may be required.

The implementation of constraints may be accomplished within the estimator formalism by Lagrange multiplier techniques (see Gubbins, 1984) or by considering the constraint equations to be data. If a non-linear constraint equation is represented as

$$G(x) = g \tag{13}$$

then the $(n+1)^{st}$ iteration relation is

$$\delta\hat{x}_{n+1} = [A^T(\hat{x}_n)\, R^{-1}A(\hat{x}_n) + \Omega_a^{-1} + C^T(\hat{x}_n)\, R_c^{-1}C(\hat{x}_n)]^{-1} \tag{14}$$

$$\cdot\, [\, A^T(\hat{x}_n)\, R^{-1}\delta y_n + \Omega_a^{-1}(\hat{x}_a - \hat{x}_n) + C^T(\hat{x}_n)\, R_c^{-1}\delta g_n]$$

where

$$C(\hat{x}_n) = \frac{\partial G}{\partial x}\bigg|_{\hat{x}_n} \tag{15}$$

$$\delta g_n = g - C(\hat{x}_n)\hat{x}_n \quad .$$

The weight matrix R_c^{-1} reflects the stiffness of the constraint, where R_c is the "covariance" matrix of the "observed" constraint. This error measure may be chosen to represent the estimated numerical precision lost in the computing process, or to represent modeling errors inherent in the constraint. This approach has also been taken by Bloxham and Gubbins (1985).

In the absence of constraints, the least squares estimation process converges rapidly (in usually no more than two iterations) when the time dependence of Gauss coefficients is a power series. In that representation, the observations of magnetic components X, Y, Z , are linear functions of the Gauss coefficients whereas the scalar field intensity, horizontal field, declination, and inclination are nonlinear functions of those parameters. While the measurements will be nonlinear functions of the parameters, they are at least, still represented in analytic form. In contrast, some of the constraints are not available in analytic form. For example, the null-curves Γ_i on which the vertical magnetic field vanishes are extremely complex functions of the model parameters and must be determined numerically. As a result numerical methods must be used to compute the matrix

$$C^T(\hat{x}_n)C(x_n)$$

for each iteration, $n = 0, 1, 2, \ldots$, until convergence is attained.

4.0 EVALUATION OF A FLUX CONSTRAINED GEOMAGNETIC FIELD MODEL

To investigate the influence of physical constraints which may be satisfied by Earth's liquid core on geomagnetic field models, we apply the non-linear algorithms described in Section 3.0 to a variation of the GSFC 12/83 model (Langel and Estes, 1985a). This model utilized quiet Magsat data and observatory annual means for a selected set of observatories for the years 1977 through 1982. The internal Gauss coefficients were expanded to degree 13 for the main terms and degree 10 for the secular variation terms. In addition to the internal Gauss coefficients, GSFC 12/83 solved for an external field of spherical harmonic degree one, and vector biases for each observatory. Moreover, parameters for linear D_{st} variation in g_{10} and the external coefficients are included in the solution. Internal coefficients which were not determined in the inversion of the data to the 95% confidence level were forced to be zero in the final solution. Because the incorporation of dynamic core constraints could improve the observability of such suppressed coefficients, the GSFC 12/83 model was recomputed with all coefficients retained in the solution and all partial derivatives included in the normal matrix $A^T R^{-1} A$. This model is designated GSFC 9/84-0 and is summarized in Table 1.

The GSFC 9/84-0 model, with the utilization of high quality Magsat data, very accurately represents the geomagnetic field at and above the Earth's surface at epoch 1980.0. Figure 1 shows the radial component of the field from GSFC 9/84-0 at the core-mantle boundary (CMB) at 1980.0, using all Gauss coefficients to degree and order thirteen. There are eleven separate null flux curves resulting from this model evaluation. Because the higher order Gauss terms, which are less well determined, become more dominant in the field evaluation at the CMB, the resulting computations are subject to large uncertainty. Benton, et.al. (1982) and Report I examined the effect of truncation level on geomagnetic properties at the CMB, and demonstrated considerable variation of null-curve location and null-patch flux as a function of degree and order. For this study, we have selected the five null-curves indicated in Figure 1 for which to impose flux constraints because these curves qualitatively demonstrated stability of form and location from truncation level nine through thirteen. Moreover, the consideration of only

five null-patches meets the objectives of the study while keeping the computational burden within reasonable bounds.

The methodology for computing the null-patch flux and the partial derivatives of the null-patch flux with respect to the model parameters (Gauss coefficients) in equation (15) is described in Report I. A numerical derivative is taken for each parameter using a $1° \times 1°$ grid overlay of the null-patch and varying the nominal Gauss coefficient value. In this approximation the field is computed at the center of each $1° \times 1°$ cell and assumed to be constant within the cell. Note that the flux depends on the constant and secular variation Gauss coefficients both through the field evaluation and the null-curve boundary, Γ_i.

For each of the five null-curves selected, we impose the "data"

$$M_i(b, t) = \text{constant}$$

from equation (4) at the times 1977.5, 1980.0, and 1982.5. Because the GSFC 9/84-0 model accurately represents the field at epoch 1980.0, we used the 1980.0 computed flux value for each null-patch to determine the constants. We are thus adding fifteen non-linear observations to the GSFC 9/84-0 data set which will influence the solution in such a way as to attempt to maintain the constancy of the flux through the five null-curves at the given epochs. The elements of the diagonal weight matrix R_c^{-1} were set to represent an error measure of 10^{-5} MWb for the "observed" flux. This value was chosen primarily by numerical experimentation to provide a stable inversion of the normal matrix.

The solution was taken through three iterations using equation (14) starting with the GSFC 9/84-0 model as the nominal starting vector for iteration one. No a priori information was assumed in the solution for the nominal model, so that Ω_a^{-1} is zero in equation (14). Each iteration was performed in two stages. The first stage processed the Magsat and observatory data set as published for GSFC 12/83 and accumulated the normal matrix

$A^T(\hat{x}_n)\ R^{-1}\ A(\hat{x}_n)$ and the vector $A^T(\hat{x}_n)\ R^{-1}\ \delta y_n$. From this information an "unconstrained" model was generated for the iteration. These models are denoted GSFC 9/84-1, GSFC 9/84-2, and GSFC 9/84-3 for iterations one, two and three, respectively. Note that for iteration one, GSFC 9/84-1 is identical to GSFC 9/84-0 since the nominal model has already been converged using the GSFC 12/83 data set. The second stage for each iteration computed the flux and flux partial derivatives for the fifteen "observations", formed the matrix $C^T(\hat{x}_n)\ R_c^{-1}\ C(\hat{x}_n)$ and the vector $C^T(\hat{x}_n)\ R_c^{-1}\ \delta g_n$, and added these to the first stage quantities to obtain the "constrained" solution for the iteration. The constrained models are denoted GSFC 9/84-1C, GSFC 9/84-2C and GSFC 9/84-3C for iterations one, two, and three, respectively.

The flux at 1977.5, 1980.0 and 1982.5 and flux rate at 1980.0 through the five null-patches for all of the models through three iterations are presented in Table 2. The maximum variation of the flux over the 1977.5 - 1982.5 interval for each patch is also given, as well as the RSS of the flux rate over all five patches. For a perfectly constrained solution, the flux rate through each null-patch should be zero. There is a clear trend showing a reduced total flux variation for the five year data interval as the solution converges. The poorest improvement is with null-curve 2, which has a maximum variation of 30 MWb for GSFC 9/84-0 and 19 MWb for GSFC 9/84-2C. Marked improvement is shown for null-curves 3, 4 and 5. The RSS of the flux rate at 1980.0 through all five patches displays a reduction from 16.1 MWb/yr to 5.9 MWb/yr.

The cost function being minimized by the estimation procedure is

$$J_{LS} = \delta y_n^T\ R^{-1}\ \delta y_n + \delta g_n^T\ R_c^{-1}\ \delta g_n \quad .$$

The first term represents the weighted sum of squares of the data misfit from the Magsat and observatory data, which we denote by Q. Table 3 presents the misfit to the Magsat and observatory data for the iterated solutions. As expected, the misfit increases with the inclusion of constraint "data". While the solution has apparently converged with respect to the Magsat data, the situation is not as clear with respect to the observatory data which is more

strongly coupled with the constraint "data" through the secular variation. Table 4 displays the compliance of the iterated solutions to the linear vorticity constraint given in equation (6).

A stern test for the validity of the null-flux approximation and the utility of including physical constraints into geomagnetic field models is the demonstration of improved model predictive capability beyond the data interval defining the model. Tables 5 - 8 display the standard deviation of fit to observatory data for the 91 observatories used in the model on a yearly basis for B, X, Y, and Z for data from 1975.5 through 1984.5. The observatory biases recovered with the solutions were included in the model evaluations, and the standard deviations were computed unweighted. The constrained models, particularly for X and Z, show a clearly improved predictive capability beyond the interval 1977.5 - 1982.5 in both directions. Within the resolution of the plots, the symbols for GSFC 9/84-3 and GSFC 9/84-3C fall directly on GSFC 9/84-2 and GSFC 9/84-2C, respectively, and consequently are not displayed. The solid vertical line at 1982.5 is to emphasize that only eight observatories were used in the solution for that year, so that the statistics for 1982.5 primarily represent predictive errors. The statistics for 1984.5 are based on a sample of only nine observatories and must be considered unreliable. The improved model prediction capability demonstrated statistically in Tables 5 through 8 has been achieved without changing the mathematical model of the secular variation. Only additional "data" have been included. This makes a strong statement for the potential usefulness of including physical constraints in field modeling.

The Gauss coefficient differences between GSFC 9/84-0 and GSFC 9/84-2C are presented in Table 9. As expected, the effect of adding flux constraints is manifest almost totally in the secular variation coefficients, with the largest influence principally in the sectorial terms. Differences between all GSFC 9/84-3C and GSFC 9/84-2C Gauss coefficients are small and show no obvious trends.

5.0 FUTURE RESEARCH PLANS

The comparison of the predictive capability of constrained and unconstrained models described in Section 4.0 demonstrates a positive improvement achieved by incorporating physical null flux constraints. This tends to support the consistency of the hypothesis that the field is frozen to the core fluid with geomagnetic observations. These results, however, are based on utilizing a limited number of null flux constraints and a limited time interval overwhich the Gauss coefficients were modeled as linear in time. To complete the analysis begun using the GSFC 12/83 model, a converged constrained model will be developed which includes the available observatory data to date (1977.5 - 1984.5) and a complete set of null flux constraints. This model will be compared with IGRF candidate models for 1985.0.

To more fully examine the influence of physical constraints in modeling secular variation, a goal for future study will be to model the main field over a longer time interval utilizing additional null flux constraint equations, and to examine the predictive error of constrained and unconstrained models. Moreover, examination of Benton's (1985) constraints on secular variation based on electromagnetism and fluid dynamics considerations offers a linear and a number of additional non-linear constraints which should be tested for compliance in unconstrained models and implemented into constrained models. Alternate representations to polynomials in time for secular variation should also be investigated.

6.0 REFERENCES

Backus, G.E. "Kinematics of secular variation in a perfectly conducting core," Phil. Trans. Roy. Soc. Lond., A263, 239 (1968).

Benton, E.R. "On fluid circulation around null-flux curves as Earth's core mantle boundary," Geophys. Astrophys. Fluid Dyn., 11, 323 (1979).

Benton, E.R. "Inviscid, frozen-flux velocity components at the top of Earth's core from magnetic observations at Earth's surface: Part 1. A new methodology," Geophys. Astrophys. Fluid Dyn., 18, 157 (1981).

Benton, E.R. "Constraints on geomagnetic secular variation modeling from electromagnetism and fluid dynamics of earth's core," First year report for NASA/Goddard Space Flight Center contract NAS5-27671, University of Colorado, 1984.

Benton, E.R. "On the coupling of fluid dynamics and electromagnetism at the top of the earth's core," submitted to Geophysical and Astrophysical Fluid Dynamics (1985).

Benton, E.R., Estes, R.H., Langel, R.A., and Muth, L.A. "Sensitivity of selected geomagnetic properties to truncation level of spherical harmonic expansions," Geophys. Res. Lett., 9, 254 (1982).

Benton, E.R., Muth, L.A., and Stix, M. "Geomagnetic contour maps at the core mantle boundary," J. Geomag. Geoelec., 31, 615 (1979).

Bloxham, J. and Gubbins, D. "Geomagnetic field analysis IV: testing the frozen flux hypothesis," Geophysical Journal (in press, 1985).

Bondi, H. and Gold, T. "On the generation of magnetism by fluid motion," Mon. Not. R. Astro. Soc., 110, 607 (1950).

Estes, R.H. "FIT program description and user's guide: Version 8305," Final Report for Contract NAS5-26486, Business and Technological Systems, Inc., BTS07-83-78, June 1983.

Estes, R.H. "Utilization of magnetohydrodynamic constraints in geomagnetic core field modeling," BTS, Inc., Final Report, NASA Contract NAS5-27672, October 1984.

Gibbs, B.P. and Estes, R.H. "Geomagnetic modeling by optimal recursive filtering," Final report for NASA/Goddard Space Flight Center contract NAS5-26250, Business and Technological Systems, 1982.

Gibbs, B.P. and Estes, R.H. "Geomagnetic field modeling errors and optimization of recursive estimation - phase I final report," NSF grant EAR-8360496, Business and Technological Systems, 1984.

Gubbins, D. "Geomagnetic field analysis - I. Stochastic inersion," Geophys. J. Roy. Astro. Soc., 73, 641 (1983).

Gubbins, D. "Geomagnetic field analysis - II. Secular variation consistent with a perfectly conducting core," Geophys. J. Roy. Astro. Soc., 77, 753 (1984).

Gubbins, D. "Finding core motions from magnetic observations," Phil. Trans. Roy. Soc. Lond. A., 306, 247 (1982).

Gubbins, D. and Bloxham, J. "Geomagnetic field analysis III: magnetic fields on the core mantle boundary," accepted for publication in the Geophys. J. Roy. Astro. Soc. (1985).

Hide, R. "How to locate the electrically-conducting core of a planet from external magnetic observations," Nature, 271, 640 (1978).

LaBrecque, J.L., Cande, S.C. and Jarrard, R.D. "The intermediate wavelength magnetic anomaly field of the North Pacific and possible source distributions," final report for NASA/Goddard Space Flight Center grant NAS5-25891, Lamont-Doherty Geological Observatory, 1982.

Langel, R.A. "The main field", Chapter 3 of Geomagnetism, J. Jacobs, editor, Academic Press, in press (1985).

Langel, R.A. and Estes, R.H. "A geomagnetic field spectrum," Geophys. Res. Lett., 9, 250 (1982).

Langel, R.A. and Estes, R.H. "The near-earth magnetic field at 1980 determined from magsat data," J. Geophys. Res., 90, No. B3, 2495 (1985a).

Langel, R.A. and Estes, R.H. "Error analysis of geomagnetic field models," Fifth General Assembly, IAGA, Prague, Czechoslovakia, August (1985b).

Langel, R.A., Estes, R.H., Fabiano, E.B., and Lancaster E.R. "Initial geomagnetic field model from MAGSAT vector data," Geophys. Res. Lett., 7, 793 (1980).

Langel, R.A., Estes, R.H., and Mead, G. D. "Some new methods in geomagnetic field modeling applied to the 1960-1980 epoch," J. Geomag. Geoelec., 34, 327 (1982).

Lowes, F.J., "Spatial power spectrum of the main geomagnetic field, and extrapolation to the core," Geophys. J. Res. Astron. Soc., 36, 717 (1974).

Luenberger, D.G., Introduction to linear and nonlinear programming, Addison-Wesley, Reading, Mass. (1973).

Malin, S.R.C. "Geomagnetic secular variation and its changes, 1942.5 to 1962.5," Geophys. J. Roy. Astron. Soc., 17, 415 (1969).

Malin, S.R.C. and Clark, A.D. "Geomagnetic secular variation, 1962.5 to 1967.5," Geophys. J. Roy. Astron. Soc., 36, 11 (1974).

Parker, R.L. and Shure, L. "Efficient modeling of the earth's magnetic field with harmonic splines," Geophys. Res. Lett., 9, 812 (1982).

Roberts, P.H. and Scott, S. "On analysis of secular variation 1.A hydromagnetic constraint: theory," J. Geomag. Geoelec., 17, 137 (1965).

Shure, L. Parker, R.L., and Backus, G.E. "Harmonic splines for geomagnetic modeling," Phys. Earth and Planet. Inter., 28, 215 (1982)

Voorhies, C.V., "Magnetic location of earth's core-mantle boundary and estimates of the adjacent fluid motion," Ph.D. thesis, University of Colorado, 1984.

Voorhies, C.V. and Benton, E.R. "Pole-strength of the earth from MAGSAT and magnetic determination of the core radius," Geophys. Res. Lett., 9, 258 (1982).

Whaler, K.A. "Geomagnetic secular variation and fluid motion at the core surface," Phil. Trans. Roy. Soc. Lond. A., 306, 235 (1982).

Table 1. MAGNETIC FIELD MODEL
GSFC 9/84-0

- **DATA SET SAME AS FOR GSFC 12/83**

  SELECTED MAGSAT VECTOR AND SCALAR DATA
  OBSERVATORY ANNUAL MEANS

YEAR	77.5	78.5	79.5	80.5	81.5	82.5
NUMBER OF OBSERVATORIES	86	91	90	90	45	8

- **GAUSS COEFFICIENTS**

  INTERNAL MAIN DEGREE 13 SV DEGREE 10
  EXTERNAL DEGREE 1
  Dst VARIATION FOR g_{10}, EXTERNAL TERMS

- **OBSERVATORY BIASES**

Table 2. SOLUTION FLUX AND FLUX RATE THROUGH NULL CURVES
MWb AND MWb/YR

Model	Null Curve	Patch 1	Max Variation |Δ|	Patch 2	Max Variation |Δ|	Patch 3	Max Variation |Δ|	Patch 4	Max Variation |Δ|	Patch 5	Max Variation |Δ|	RSS of Flux Rate
GSFC 9/84-0												
Flux	77.5	-17454		1410		156		-37		53		
	80.0	-17449		1386		131		-56		40		
	82.5	-17488		1380		107		-77		32		
Flux Rate	80.0	-6.9	39	-5.7	30	-10.0	49	-8.0	40	-3.8	21	16.1
GSFC 9/84-1C												
Flux	77.5	-17456		1408		133		-56		41		
	80.0	-17443		1391		127		-52		38		
	82.5	-17472		1405		133		-56		40		
Flux Rate	80.0	-2.4	29	-0.1	17	-0.1	6	-0.2	4	-0.1	3	2.4
GSFC 9/84-2												
Flux	77.5	-17448		1408		142		-38		54		
	80.0	-17440		1392		128		-55		40		
	82.5	-17452		1388		119		-74		28		
Flux Rate	80.0	-0.6	12	-3.8	20	-4.6	23	-7.4	36	-5.4	26	10.9
GSFC 9/84-2C												
Flux	77.5	-17453		1400		125		-47		42		
	80.0	-17444		1390		128		-54		42		
	82.5	-17437		1396		133		-62		44		
Flux Rate	80.0	5.5	16	-1.0	10	1.8	8	-3.2	15	0.5	2	6.7
GSFC 9/84-3												
Flux	77.5	-17448		1408		141		-38		54		
	80.0	-17439		1392		129		-55		40		
	82.5	-17451		1388		118		-74		27		
Flux Rate	80.0	-0.7	12	-3.8	20	-4.7	23	-7.4	36	-5.5	27	11.0
GSFC 9/84-3C												
Flux	77.5	-17436		1405		127		-61		40		
	80.0	-17438		1389		130		-56		41		
	82.5	-17450		1386		136		-54		41		
Flux Rate	80.0	-4.0	14	-3.7	19	1.9	9	1.3	7	0.2	1	5.9

Table 3. COST FUNCTION EVALUATION

MODEL	MAGSAT (54,813 OBSERVATIONS)		OBSERVATORY (972 OBSERVATIONS)		TOTAL Q
	Q	RMS OF ALL DATA (nT)	Q	RMS OF X, Y, Z (nT)	
GSFC 984-0	22,332	6.38	5891	14.3 4.6 5.9	28,223
GSFC 984-2	20,916	6.17	5605	14.1 4.6 5.4	26,521
GSFC 984-2C	21,065	6.20	5799	14.3 4.5 5.7	26,864
GSFC 984-3	20,916	6.17	4239	11.2 4.5 6.2	25,155
GSFC 984-3C	21,060	6.19	4309	11.0 4.6 6.6	25,369

Table 4. LINEAR VORTICITY CONSTRAINT COMPLIANCE

MODEL	$\dot{L}_E$ AT 1980
GSFC 12/83	-11.6
GSFC 9/84-0	-37.6
GSFC 9/84-2	-12.3
GSFC 9/84-2C	36.4
GSFC 9/84-3	-12.4
GSFC 9/84-3C	4.0

TABLE 5

Variation of σ_B with Time (Unweighted) for Observatory Annual Means Including Model Anomalies

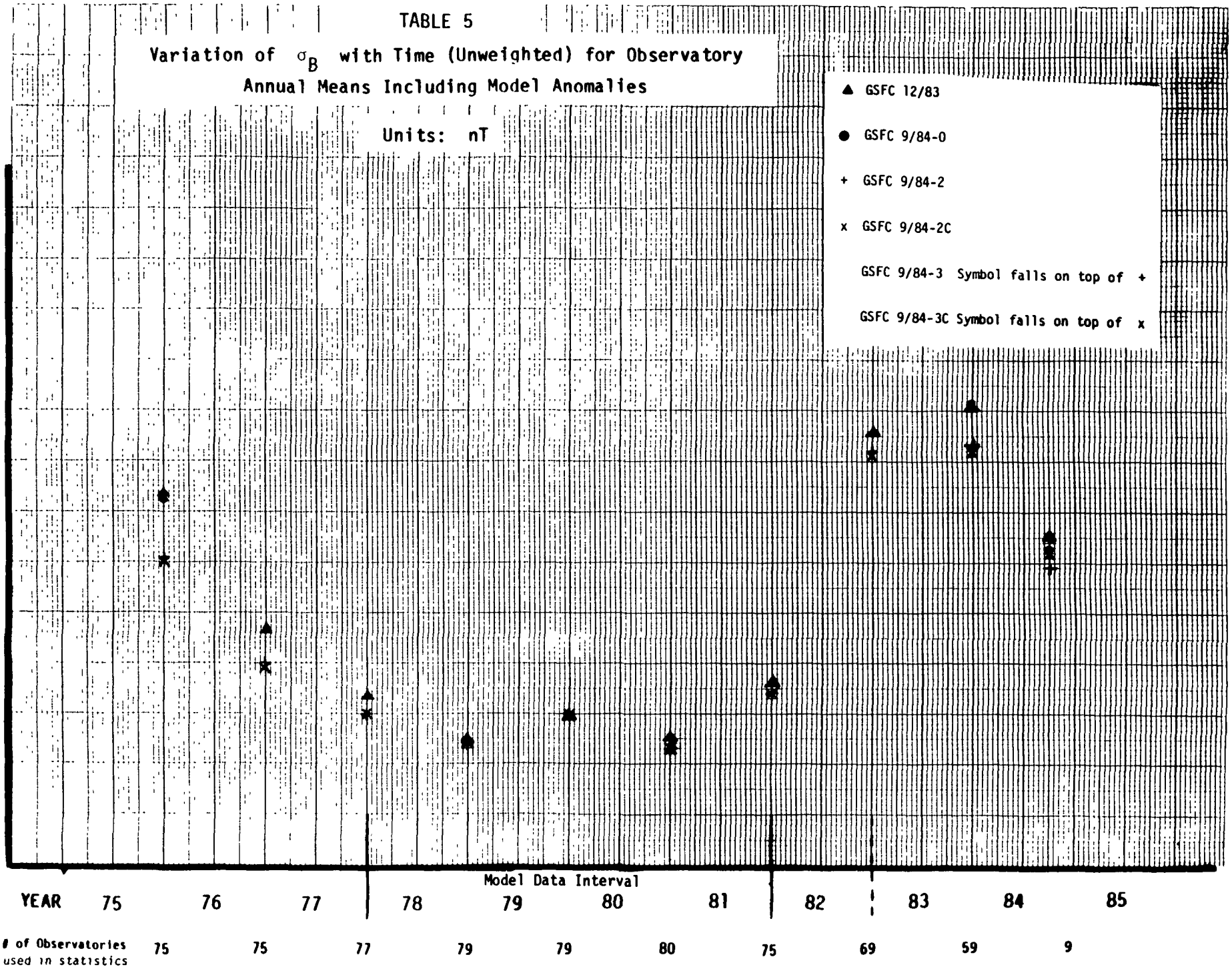

TABLE 6

Variation of σ_X with Time (Unweighted) for Observatory Annual Means Including Model Anomalies

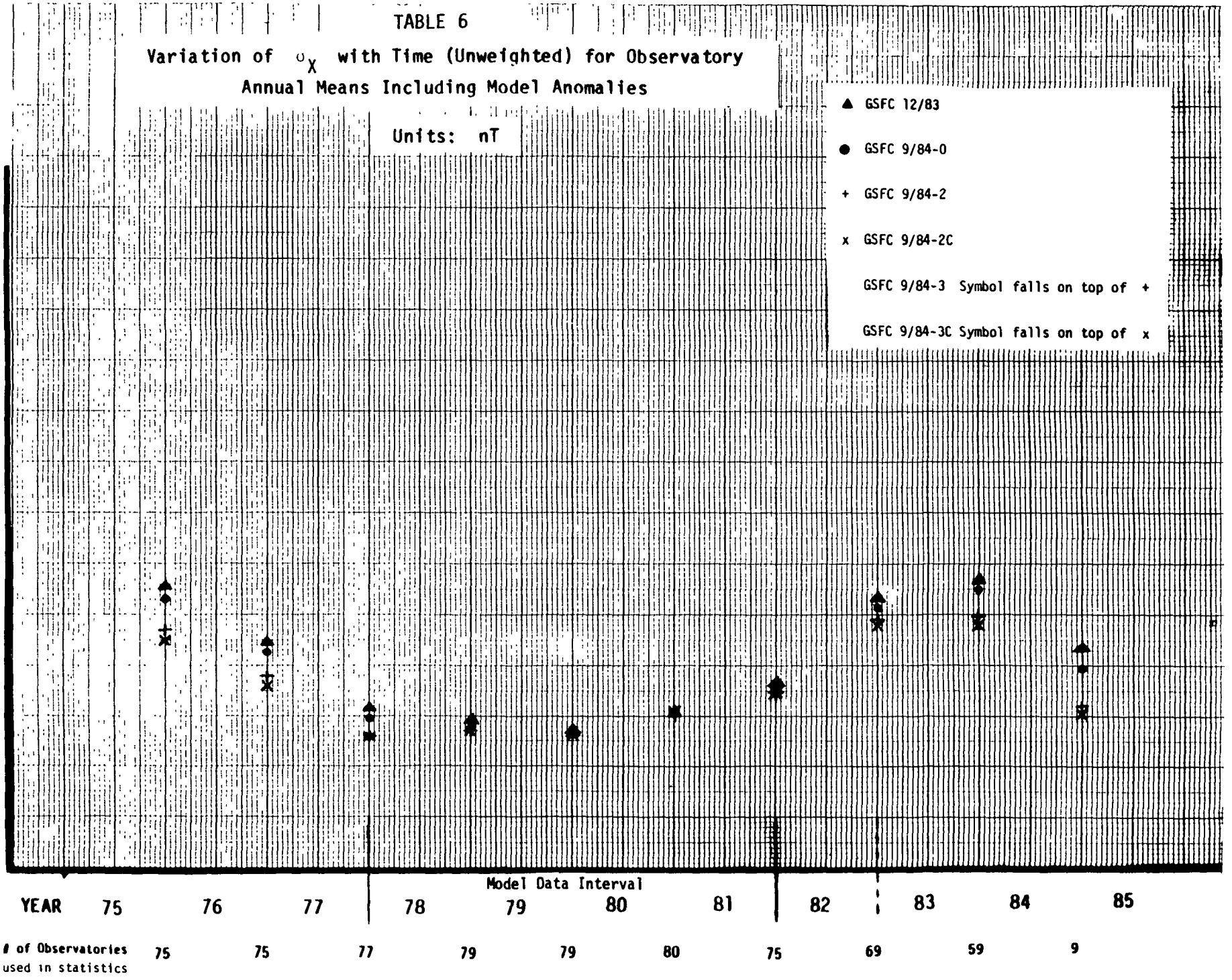

TABLE 7

Variation of σ_Y with Time (Unweighted) for Observatory Annual Means Including Model Anomalies

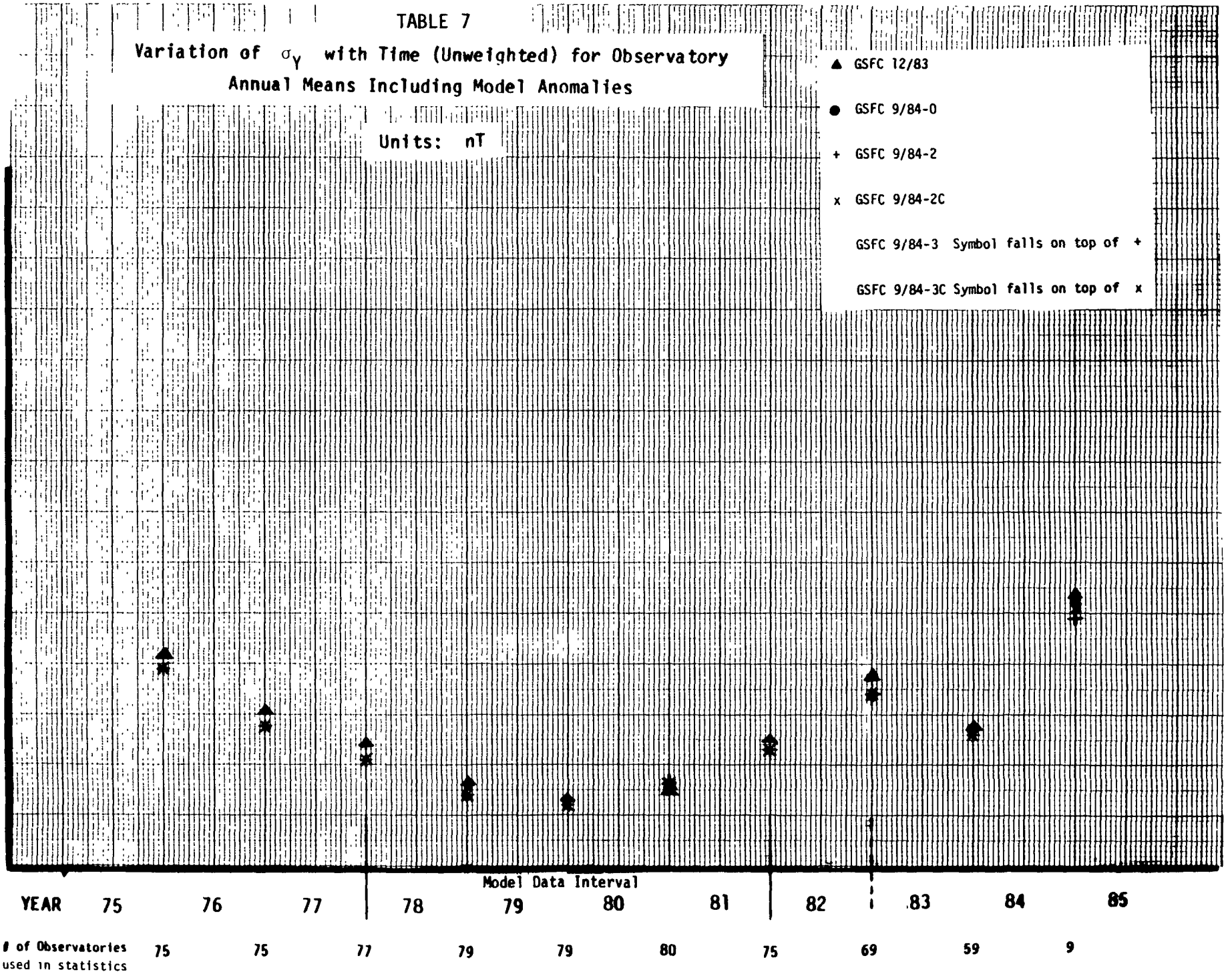

TABLE 8

Variation of σ_Z with Time (Unweighted) for Observatory Annual Means Including Model Anomalies

Units: nT

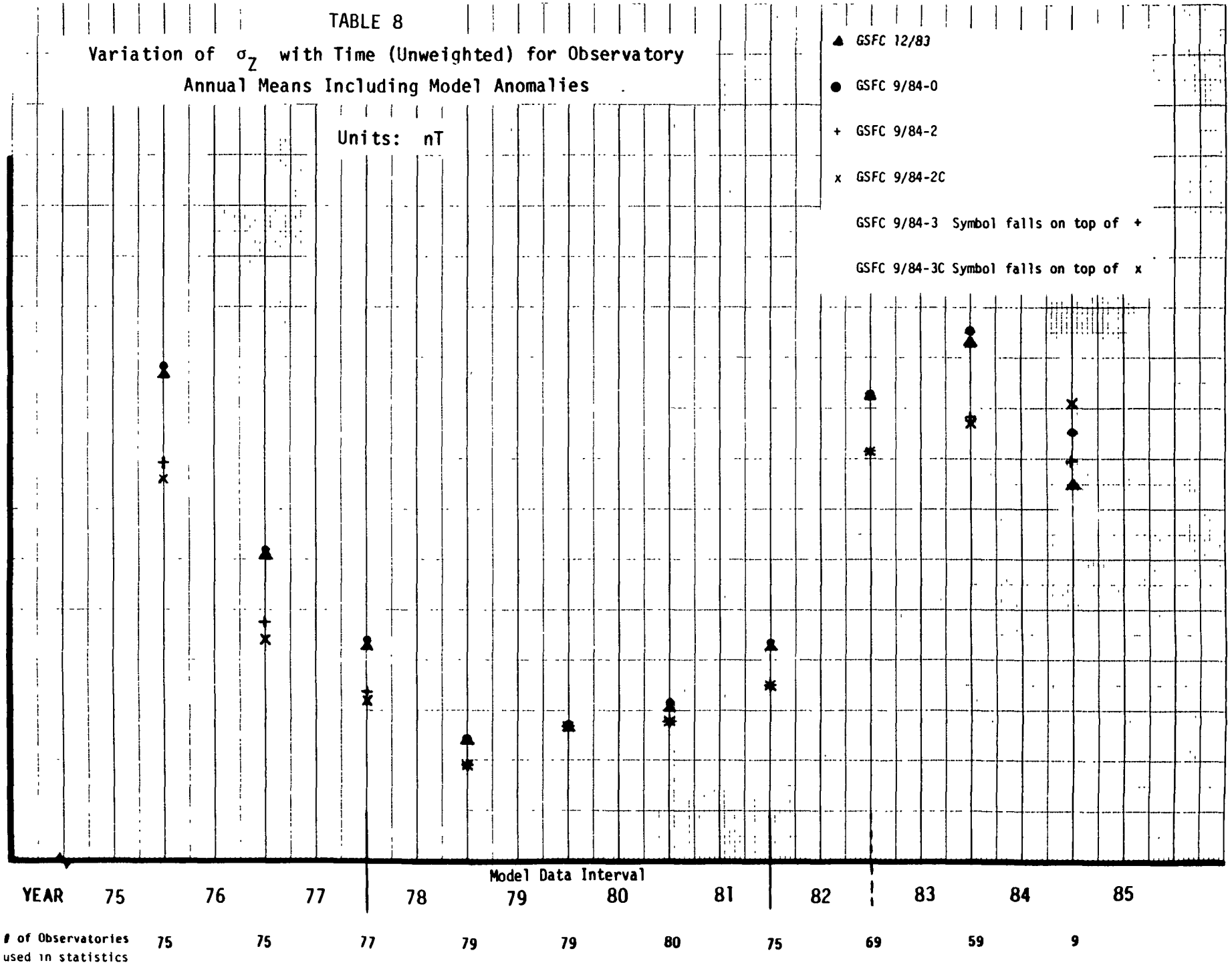

Table 9. GAUSS COEFFICIENT DIFFERENCES
GSFC 9/84-0 MINUS GSFC 9/84-2C

DIFFERENCED MODELS

n+1	m+1	g_{nm}	h_{nm}	$\dot{g}_{nm}$	$\dot{h}_{nm}$
2	1	-0.50	0.0	1.40	0.0
2	2	0.01	-0.19	-0.47	1.21
3	1	-0.03	0.0	0.05	0.0
3	2	0.02	0.15	0.04	-0.69
3	3	0.10	-0.03	-1.22	0.58
4	1	-0.08	0.0	-1.26	0.0
4	2	0.20	-0.25	1.17	-0.37
4	3	0.16	-0.19	0.73	-0.07
4	4	0.05	0.44	1.19	3.75
5	1	0.11	0.0	0.29	0.0
5	2	0.17	-0.28	-0.22	-0.52
5	3	0.55	-0.02	1.09	-0.56
5	4	0.18	-0.19	-1.28	-1.73
5	5	0.51	-0.01	3.05	-1.41
6	1	0.04	0.0	-0.27	0.0
6	2	0.00	0.05	-0.08	-0.28
6	3	0.03	-0.01	-0.42	0.35
6	4	0.06	0.06	-0.65	-0.79
6	5	0.13	-0.03	-1.35	0.35
6	6	0.03	0.06	0.04	-0.81
7	1	-0.07	0.0	0.66	0.0
7	2	-0.01	-0.06	-0.02	0.66
7	3	0.03	-0.07	-0.72	0.61
7	4	-0.04	-0.06	0.50	0.60
7	5	-0.03	-0.07	0.65	0.29
7	6	-0.02	-0.08	0.15	0.71
7	7	-0.13	0.00	1.07	-0.34
8	1	-0.05	0.0	0.78	0.0
8	2	-0.01	0.03	-0.01	-0.35
8	3	0.00	-0.03	0.15	0.45
8	4	0.01	-0.02	0.04	0.32
8	5	0.05	0.07	-0.29	-0.59
8	6	0.12	0.02	-1.20	0.03
8	7	0.03	-0.05	-0.17	0.34
8	8	-0.10	0.09	1.34	-0.64
9	1	0.06	0.0	-0.61	0.0
9	2	-0.01	0.04	0.10	-0.34
9	3	-0.04	0.03	0.60	-0.32
9	4	-0.00	-0.01	-0.17	0.05
9	5	0.05	0.01	-0.58	-0.06
9	6	0.01	-0.04	-0.18	0.40
9	7	0.00	0.02	-0.18	-0.19
9	8	-0.00	-0.05	-0.08	0.57
9	9	0.07	0.23	-0.75	-2.22
10	1	0.03	0.0	-0.16	0.0
10	2	0.01	-0.01	-0.04	0.20
10	3	0.00	0.04	-0.09	-0.31
10	4	-0.00	0.02	-0.03	-0.23
10	5	-0.02	-0.04	0.05	0.51
10	6	-0.05	0.06	0.48	-0.42
10	7	-0.05	-0.02	0.44	0.18
10	8	0.05	-0.02	-0.52	0.03
10	9	-0.05	-0.08	0.43	0.78
10	10	0.11	-0.16	-1.06	1.79

DIFFERENCED MODELS

n+1	m+1	g_{nm}	h_{nm}	$\dot{g}_{nm}$	$\dot{h}_{nm}$
11	1	-0.06	0.0	0.63	0.0
11	2	-0.01	0.05	0.15	-0.40
11	3	0.03	-0.05	-0.21	0.24
11	4	-0.00	-0.03	-0.00	0.10
11	5	0.01	0.04	-0.15	-0.37
11	6	-0.04	0.02	0.57	-0.15
11	7	-0.02	-0.02	0.02	0.12
11	8	0.01	0.03	-0.23	-0.33
11	9	-0.04	-0.03	0.45	0.33
11	10	-0.01	0.06	0.01	-0.47
11	11	-0.00	0.00	-0.05	-0.03
12	1	0.02	0.0	0.0	0.0
12	2	-0.02	-0.01	0.0	0.0
12	3	0.00	0.00	0.0	0.0
12	4	0.00	0.01	0.0	0.0
12	5	0.00	-0.00	0.0	0.0
12	6	-0.01	0.01	0.0	0.0
12	7	0.01	0.02	0.0	0.0
12	8	0.03	0.01	0.0	0.0
12	9	0.02	-0.00	0.0	0.0
12	10	0.02	-0.00	0.0	0.0
12	11	-0.01	0.02	0.0	0.0
12	12	0.02	0.01	0.0	0.0
13	1	-0.02	0.0	0.0	0.0
13	2	0.02	-0.02	0.0	0.0
13	3	0.00	-0.01	0.0	0.0
13	4	-0.00	0.00	0.0	0.0
13	5	-0.01	-0.00	0.0	0.0
13	6	0.00	0.02	0.0	0.0
13	7	0.01	-0.01	0.0	0.0
13	8	0.01	0.01	0.0	0.0
13	9	0.02	0.01	0.0	0.0
13	10	0.02	-0.00	0.0	0.0
13	11	0.01	0.02	0.0	0.0
13	12	-0.00	-0.03	0.0	0.0
13	13	-0.01	-0.01	0.0	0.0
14	1	0.03	0.0	0.0	0.0
14	2	-0.02	0.00	0.0	0.0
14	3	0.04	-0.00	0.0	0.0
14	4	-0.01	0.02	0.0	0.0
14	5	0.01	-0.01	0.0	0.0
14	6	0.02	-0.02	0.0	0.0
14	7	0.01	0.01	0.0	0.0
14	8	0.02	0.01	0.0	0.0
14	9	0.01	-0.00	0.0	0.0
14	10	-0.01	0.00	0.0	0.0
14	11	0.01	-0.01	0.0	0.0
14	12	-0.05	0.01	0.0	0.0
14	13	-0.07	-0.07	0.0	0.0
14	14	0.05	0.04	0.0	0.0

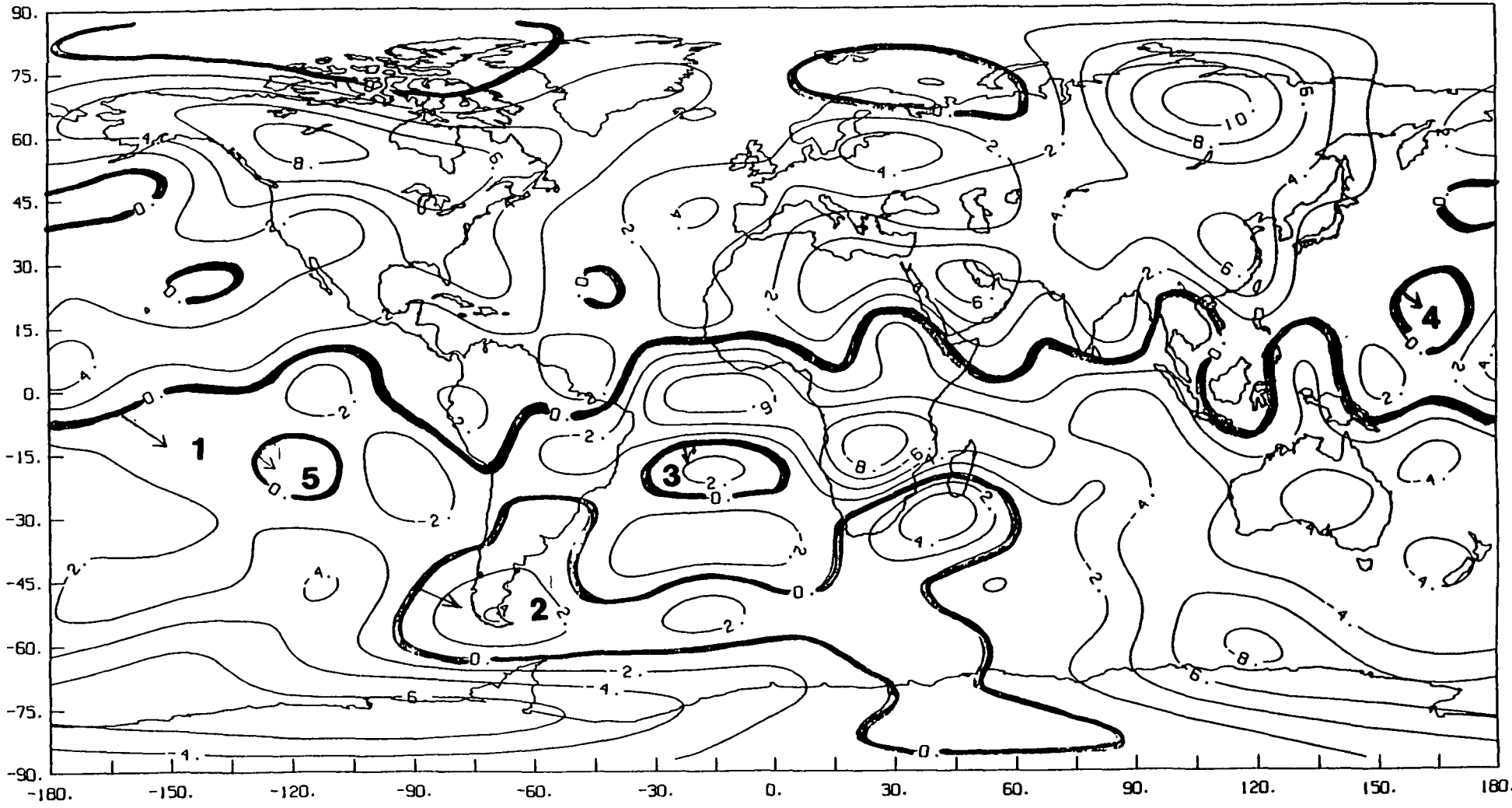

GSFC 9/84-0 $Z = -B_r$ Component at CMB at 1980

Units: Gauss (10^5 nT)

FIGURE 1

BTS BUSINESS AND TECHNOLOGICAL SYSTEMS, INC.
AEROSPACE BUILDING, SUITE 440
10210 GREENBELT ROAD • SEABROOK, MARYLAND 20706 • 301/794-8800